Transient fluid forces on a rigid circular cylinder subjected to small-amplitude motions

Cédric Leblond, Vincent Mélot, Jean-François Sigrist, Christian Lainé, Bruno Auvity, Hassan Peerhossaini

Transient Fluid Forces on a Rigid Circular Cylinder Subjected to Small Amplitude Motions

Cédric Leblond, Vincent Melot, Jean-François Sigrist, Christian Lainé

DCNS Propulsion, Service Technique et Scientifique, 44620 La Montagne, France

Bruno Auvity, Hassan Peerhossaini

Laboratoire de Thermocinétique, CNRS UMR 6607, Rue Christian Pauc, BP 50609,44306 Nantes, France

The present paper treats the transient fluid forces experienced by a rigid circular cylinder moving along a radial line in a fluid initially at rest. The body is subjected to a rapid displacement of relatively small amplitude in relation to its radius. Both infinite and cylindrically confined fluid domains are considered. Furthermore, non-negligible ampli-tude motions of the inner cylinder, and viscous and compressible fluid effects are ad-dressed, successively. Different analytical methods and models are used to tackle each of these issues. For motions of non-negligible amplitude of the inner cylinder, a potential flow is assumed and the model, formulated as a two-dimensional boundary perturbation problem, is solved using a regular expansion up to second order. Subsequently, viscous and compressible effects are handled by assuming infinitesimal amplitude motions. The viscous fluid forces are formulated by solving a singular perturbation problem of the first order. Compressible fluid forces are then determined from the wave equation. A nonlinear formulation is obtained for the non-negligible amplitude motion. The viscous and com-pressible fluid forces, formulated in terms of convolution products, are linked to fluid history effects induced by wave propagation phenomena in the fluid domain. These mod-els are expressed with dimensionless parameters and illustrated for a specific motion imposed on the inner cylinder. The different analytical models permit coverage of a broad range of motions. Hence, for a given geometry and imposed displacement, the appropriate fluid model can be identified and the resulting fluid forces rapidly estimated. The limits of these formulations are also discussed.

Keywords: circular cylinder, shock loading, transient dynamics, analytical method, fluid forces, history effect, confinement effect

1 Introduction

In the case of shock loading that results from underwater explosion, naval propulsion devices can be subjected to highly accelerated, high frequency motions. These components can be in contact with a fluid, which is the case for heat exchangers, nuclear propulsion reactors, or squeeze-film dampers. In order to improve design margins and ensure safety, long life, and satisfactory operating performance of the shock loaded components, the precise knowledge of the fluid effects on the solid components is of major importance. Since the body motion modifies the fluid flow, and the fluid flow influences the body motion, complex fluid/structure interaction problems have to be accounted for. In order to choose an appropriate fluid model, design engineers must identify the meaningful physical phenomena occurring in their particular geometry. This can be done by estimating the fluid forces on simplified representative geometries, for which analytical results are available.

The purpose of the present paper is to formulate and group such models for a rigid circular cylinder subjected to relatively small amplitude transient motions along a radial line, in an annular or infinite fluid domain. Numerous analytical and numerical methods are now available for the harmonic dynamics of this geometry [1,2]. It also continues to be an active domain of interest particularly to studies of flow-induced vibrations. However, transient dynamics have comparatively received little attention. Although the solution of a time-dependent problem can be obtained from the solution of the corresponding harmonic problem using Fourier synthesis methods or series of resonance modes [3,4], time-domain methods can provide more physical insight. Such methods are currently receiving considerable attention [5–8], in particular, due to increasing computer capabilities and constantly improving computational methods.

This paper deals with several aspects of fluid effects in one of the simplest two-dimensional fluid problems, illustrated in Fig. 1. The motion of the inner cylinder is imposed and the outer cylinder, when present, is fixed. Consequently, this is not a fluid-structure interaction problem and emphasis can be especially placed on the forces acting on the moving cylinder. Highly confined flows, such as those encountered in squeeze-film dampers or rotating machinery, are not discussed here. Related fluid effects can be found in other articles [9–14]. In this study, the imposed motion is assumed sufficiently small, that no boundary-layer separation occurs [15]. Hence, there is neither wake formation nor its force related modifications [16,17]. Two-phase flows are also not considered. Some elements concerning the associated damping effect can be found in a review article [18].

The problem of interest is governed by seven independent dimensional parameters: R_1, R_2, ρ, ν, c, U, and ω. R_1 and R_2 are the geometrical parameters denoting the inner and outer cylinder radii, respectively; ρ, ν, and c are the fluid parameters representing the density, the kinematic viscosity, and the speed of sound in the fluid at rest. Lastly, U and ω denote the characteristic velocity and pulsation frequency of the imposed inner motion. For instance, U may be the maximum velocity and ω the pulsation with the maximum energy in the power spectrum of the transient motion. Since there are three fundamentals units, length, mass and time, the problem is driven by four independent dimensionless numbers. While there are of course infinite ways to build such numbers

[1]Corresponding author.

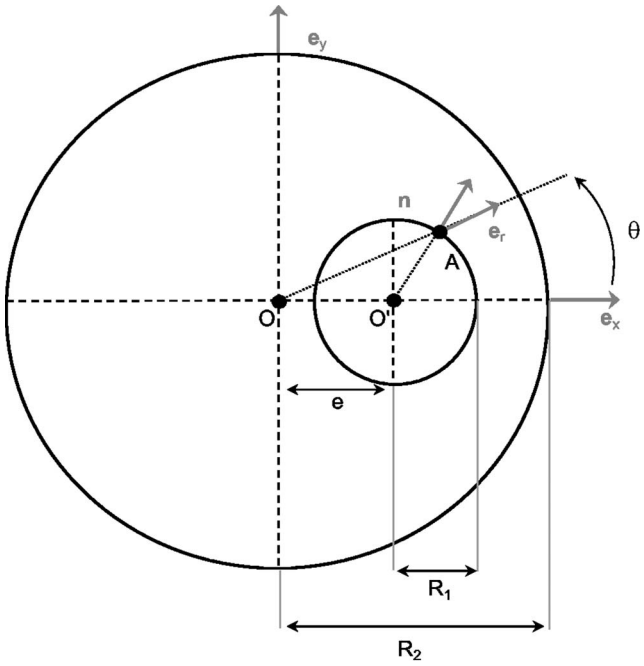

Fig. 1 Geometrical configuration

from the seven dimensional numbers, it will be seen below that the four following ones are particularly meaningful:

$$\alpha = \frac{R_2}{R_1}, \quad \lambda = \frac{U}{R_1\omega}, \quad \beta = \frac{R_1^2\omega}{\nu}, \quad \Omega = \frac{R_1\omega}{c} \tag{1}$$

Here, α is the dimensionless geometrical parameter called the confinement number. λ, often called the Keulegan–Carpenter number, quantifies the displacement of the inner cylinder in relation to its radius and takes into account fluid advection and geometrical deformation. β, the Stokes number, is the ratio between unsteady and viscous effects, and Ω is used to take into account the fluid compressibility in unsteady flows.

Section 2 of this paper considers motions of non-negligible amplitude in an incompressible and inviscid flow. The problem is formulated as a boundary-perturbation method for the velocity potential and a regular expansion is used to solve it up to the second order. Hence, fluid advection and geometrical deformations due to the inner motion are approximately taken into account. The resulting fluid force expression depends nonlinearly on the imposed instantaneous displacement, velocity, and acceleration, and can be seen as an extension of the Fritz model [19], which is limited to very small amplitude motions. Its dimensionless formulation highlights the Keulegan–Carpenter number as the meaningful parameter in quantifying large-displacement effects. In Sec. 3, the fluid viscosity is considered assuming a small amplitude imposed motion that is rapid enough that the boundary layer thickness can be taken as much less than the radial clearance. The corresponding fluid forces are obtained using a singular perturbation method solved at the first order. Its expression includes a convolution product whose amplitude is quantified by the Stokes number. Section 4 takes fluid compressibility into account, assuming a small amplitude motion and inviscid flow. The forces are derived by solving the wave equation for the velocity potential and take the form of a convolution product whose kernel depends on the compressibility number. The viscous and compressible fluid force expressions extend the harmonic models of Chen [2] for transient motions. In Sec. 5, the fluid forces obtained using these models are illustrated and compared for a specific imposed inner-cylinder motion.

2 Motion of Non-Negligible Amplitude in a Potential Flow

2.1 General Equations. Here, a rapidly moving circular cylinder in a two-dimensional annular incompressible and inviscid fluid region is considered. The fluid forces on the inner cylinder for an infinitesimal displacement are found in Ref. [19], in which fluid advection and geometrical deformation are neglected. An extension of this model to larger amplitude motions is proposed by formulating the problem as a boundary-perturbation problem [20] solved up to the second order. Only the main steps of the derivation are described here; a more detailed account can be found in Ref. [21]. Another way of accounting for large-displacement effects can be found in Refs. [13,14]. In this section, the fluid forces are obtained by solving the dimensional equations and are then expressed in a dimensionless form at the end.

Since the flow is assumed inviscid and initially irrotational, it remains irrotational at later times [22] and can be described by the Laplace equation for the velocity potential Φ as follows:

$$\nabla^2\Phi = 0 \tag{2}$$

The normal component of the fluid velocity at the boundaries must equal the velocity of the cylinders, so that the boundary conditions can be written as

$$\nabla\Phi \cdot \mathbf{e_r} = 0 \quad \text{on the fixed outer cylinder} \tag{3}$$

$$\nabla\Phi \cdot \mathbf{n} = \dot{e}(t)\mathbf{e_x} \cdot \mathbf{n} \quad \text{on the moving inner cylinder} \tag{4}$$

where $\dot{e}(t)$ is the inner-cylinder velocity, $\mathbf{e}_x$ the unit vector along the x-axis, and $\mathbf{n}$ the unit outward normal, as illustrated in Fig. 1. In order to make this problem analytically tractable, the position of the inner cylinder and the unit normal in Eq. (4) must be explicitly expressed.

2.2 Boundary-Perturbation Formulation. By considering the triangle $OO'A$ in Fig. 1, the position of the inner circular cylinder $\mathcal{C}(t)$ can be characterized by the polar equation

$$r_c(\theta,t) = e(t)\cos\theta + R_1\sqrt{1 - \frac{e^2(t)}{R_1^2}\sin^2\theta} \tag{5}$$

where $e(t)$ is the inner-cylinder displacement. This formula is only valid for $|e(t)/R_1| < 1$. Expanding the square root in terms of series gives the relation

$$r_c(\theta,t) = R_1\left\{1 + \cos\theta\frac{e(t)}{R_1} + \sum_{n=1}^{\infty}(-1)^n(\sin\theta)^{2n}\frac{1}{n!}\prod_{k=0}^{n-1}\left(\frac{1}{2}-k\right) \times\left[\frac{e(t)}{R_1}\right]^{2n}\right\} \tag{6}$$

By introducing the perturbation parameter $\varepsilon(t)$,

$$\varepsilon(t) = \frac{e(t)}{R_1} \tag{7}$$

approximate positions of the inner cylinder can be evaluated at a given order in powers of $\varepsilon(t)$. Hence, by neglecting third-order terms and higher in Eq. (6), the second-order approximation for the inner-cylinder position takes the form

$$r_c(\theta,t) \approx R_1[1 + \varepsilon(t)\cos\theta - \tfrac{1}{2}\varepsilon^2(t)\sin^2\theta] \tag{8}$$

It is also useful to write in explicit terms the unit outward normal $\mathbf{n}$ on the moving inner cylinder so as to express the boundary condition (4). Thus, the parametric curve Ψ of $\mathcal{C}(t)$ is introduced as follows:

$$\mathcal{C}(t): \theta \mapsto \Psi(\theta) = \mathcal{O} + r_c(\theta,t)\mathbf{e_r}(\theta,t) \tag{9}$$

where $\mathcal{O}$ denotes the center of the outer cylinder. The unit tangent $\mathbf{T}$ to $\mathcal{C}(t)$ at the position θ is given by:

$$\mathbf{T}(\theta) = \frac{\Psi'(\theta)}{\|\Psi'(\theta)\|} \tag{10}$$

with

$$\Psi'(\theta) = r_c'(\theta)\mathbf{e_r} + r_c(\theta)\mathbf{e}_\theta \tag{11}$$

The prime denotes a derivative according to θ. The unit normal $\mathbf{n}$ orthogonal to $\mathbf{T}$ can then be evaluated. Its truncation at the second order in powers of $\varepsilon(t)$ is

$$\mathbf{n}(\theta,t) \approx \frac{R_1}{\|\Psi'(\theta)\|}\left[\cos\theta + \varepsilon(t)\cos 2\theta - \frac{3}{8}\varepsilon^2(t)(\cos\theta - \cos 3\theta)\right]\mathbf{e_x} + \frac{R_1}{\|\Psi'(\theta)\|}\left[\sin\theta + \varepsilon(t)\sin 2\theta - \frac{3}{8}\varepsilon^2(t)(\sin\theta - \sin 3\theta)\right]\mathbf{e_y} \tag{12}$$

The boundary condition on the moving inner cylinder (4) can now be seen as the extreme boundary condition of the following family:

$$\nabla\Phi[r_n(\theta,t),\theta]\cdot\mathbf{n}[r_n(\theta,t),\theta] = \dot{e}(t)\mathbf{e_x}\cdot\mathbf{n}[r_n(\theta,t)\theta] \tag{13}$$

where $r_n(\theta,t)$ is the nth-order approximation of the power series expansion of the inner-cylinder position $r_c(\theta,t)$. Performing a Taylor expansion of Eq. (13) about R_1 permits turning the original problem into an equivalent sequence of problems with solutions Φ_0, Φ_1, Φ_2, Φ_3,… that can be found recursively. Each Φ_n must satisfy the following Laplace equation and outer boundary condition:

$$\frac{\partial^2\Phi_n}{\partial r^2} + \frac{1}{r}\frac{\partial\Phi_n}{\partial r} + \frac{1}{r^2}\frac{\partial^2\Phi_n}{\partial\theta^2} = 0 \tag{14}$$

$$\left.\frac{\partial\Phi_n}{\partial r}\right|_{r=R_2} = 0 \tag{15}$$

Due to Eqs. (8), (12), and (13) and several Taylor expansions, the boundary conditions on the inner cylinder up to the second order are given by

$$\left.\frac{\partial\Phi_0}{\partial r}\right|_{r=R_1} = \dot{e}(t)\cos\theta \tag{16}$$

$$\left.\frac{\partial\Phi_1}{\partial r}\right|_{r=R_1} = \frac{2\alpha^2}{\alpha^2-1}\dot{e}(t)\cos 2\theta \tag{17}$$

$$\left.\frac{\partial\Phi_2}{\partial r}\right|_{r=R_1} = \frac{2\alpha^2}{(\alpha^2-1)^2(\alpha^2+1)}\dot{e}(t)\cos\theta + \frac{3\alpha^2(\alpha^4+1)}{(\alpha^2-1)^2(\alpha^2+1)}\dot{e}(t)\cos 3\theta \tag{18}$$

where Eqs. (17) and (18) are anticipated knowledge of the solutions Φ_0 and Φ_1, respectively. Hence, each Φ_n is the solution of the Laplace equation on a fixed annular fluid region with Neumann boundary conditions. The solution of the general problem is then achieved using

$$\Phi = \sum_{n=0}^{\infty}\varepsilon^n(t)\Phi_n \tag{19}$$

If the perturbation parameter is sufficiently small, the series will converge rapidly and a few terms will suffice for a good approximation of the solution.

2.3 Fluid Forces Evaluation. The results are obtained up to the second order, so the solution is expected to be valid in cases where $[e(t)/R_1]^3 \ll 1$. Here, Φ_0, Φ_1, and Φ_2 are found by solving Eqs. (14)–(18) by separation of variables. Their expressions can be found in Ref. [21]. Once the velocity potential is determined, the pressure in the fluid domain can be obtained from the Bernoulli relation [22]

$$p = -\rho\frac{\partial\Phi}{\partial t} - \rho\frac{1}{2}(\nabla\Phi)^2 + C \tag{20}$$

where ρ is the fluid density and C a constant available in the whole fluid domain. Since the flow is assumed inviscid, the integrated fluid forces per unit length on the moving inner circular cylinder can be written as

$$\mathbf{F}(t) = -\int_0^{2\pi} p(r_c(\theta,t))\bar{\bar{I}}\cdot\mathbf{n}(\theta,t)\|\Psi'(\theta)\|\mathrm{d}\theta \tag{21}$$

with $\bar{\bar{I}}$ the identity matrix. By performing Taylor expansions about $r=R_1$ in the pressure term of the above equation, the fluid forces up to the second order can be found. Only the $\mathbf{e_x}$-direction component of $\mathbf{F}$ is nonzero and its dimensional expression is given by

$$\varphi(t) = -\rho\pi R_1^2\frac{\alpha^2+1}{\alpha^2-1}\ddot{e}(t) + \rho\pi\frac{2\alpha^2}{(\alpha^2-1)^3(\alpha^2+1)}e(t)\dot{e}^2(t) - \rho\pi\frac{4\alpha^4}{(\alpha^2-1)^3(\alpha^2+1)}e^2(t)\ddot{e}(t) \tag{22}$$

The first term on the right-hand side, which is the main-order term, is exactly the Fritz model [19]. It is proportional to the inner-cylinder acceleration and consists only in an added mass effect. The next two terms are displacement-dependent nonlinear corrections. The first one, proportional to the square of the inner-cylinder velocity, is induced by the fluid advection, and the second one can be seen as an added mass induced by relatively large amplitude motions. For an infinite fluid domain ($\alpha\to\infty$), the force expression reduces to $-\rho\pi R_1^2\ddot{e}(t)$, the well-known fluid displaced term. It is fruitful to express the fluid forces with dimensionless quantities. By normalizing t, $e(t)$, $\dot{e}(t)$, $\ddot{e}(t)$, and $\varphi(t)$ according to Table 1, the resulting second-order nondimensional fluid forces can be written as

$$\varphi(t) = -\frac{\alpha^2+1}{\alpha^2-1}\ddot{e}(t) + \lambda^2\frac{2\alpha^2}{(\alpha^2-1)^3(\alpha^2+1)}[e(t)\dot{e}^2(t) - 2\alpha^2e^2(t)\ddot{e}(t)] \tag{23}$$

The Keulegan–Carpenter number λ appears explicitly and allows quantification of the large-displacement nonlinear effects.

Table 1 Normalization factors for the variables

Variable	Normalization factor
Length	R_1
Time	$1/\omega$
Velocity	U
Displacement	U/ω
Acceleration	$U\omega$
Potential	R_1U
Pressure	$\rho R_1U\omega$
Force	$\rho\pi R_1^2U\omega$

3 Viscous Model

3.1 Problem Formulation. Small amplitude motions of the inner-circular cylinder in a viscous incompressible fluid are now addressed. For an infinite fluid domain, the harmonic problem was solved by Stokes [23]. An approximate solution is proposed here for transient motion in a confined flow that is achieved using a matched asymptotic expansion at first order, also known as the composite boundary-layer solution [15]. The incompressible

Navier–Stokes equations are the starting point. All variables are normalized as indicated in Table 1. The nondimensional governing equations take the form

$$\frac{\partial \mathbf{u}}{\partial t} + \lambda(\mathbf{u}\cdot\nabla)\mathbf{u} = -\nabla p + \beta^{-1}\nabla^2\mathbf{u} \tag{24}$$

$$\nabla\cdot\mathbf{u} = 0 \tag{25}$$

where $\mathbf{u}$ denotes the fluid velocity and p the pressure. The Keulegan–Carpenter number λ and the Stokes number β appear explicitly. Since a small amplitude motion in relation to the inner-cylinder radius is assumed here, the Keulegan–Carpenter number is small and the advection term can be neglected. Moreover, the no-slip boundary conditions can then be applied on fixed boundaries as follows:

$$\mathbf{u}|_{r=1} = \dot{e}(t)\mathbf{e}_\mathbf{x}, \quad \mathbf{u}|_{r=\alpha} = 0 \tag{26}$$

The inner-cylinder motions are also assumed to be rapid enough that the viscous boundary layer will be much smaller than the radial clearance. Hence, the fluid domain can be divided into two parts: one far from the boundaries, where viscous effects can be neglected, and the other closer to the boundaries, where the viscous dissipation is a main-order term [24].

3.2 Outer Resolution. Far from the boundaries, the following outer expansion in $\beta^{-1/2}$ is introduced into the nondimensional Navier–Stokes equations:

$$\begin{pmatrix}\mathbf{u}(r,\theta,t)\\ p(r,\theta,t)\end{pmatrix} = \begin{pmatrix}\mathbf{u}_0(r,\theta,t)\\ p_0(r,\theta,t)\end{pmatrix} + \beta^{-1/2}\begin{pmatrix}\mathbf{u}_1(r,\theta,t)\\ p_1(r,\theta,t)\end{pmatrix} + \mathcal{O}(\beta^{-1}) \tag{27}$$

Keeping only the main-order terms gives

$$\partial_t\mathbf{u}_0 = -\nabla p_0 \tag{28}$$

$$\nabla\cdot\mathbf{u}_0 = 0 \tag{29}$$

Since Eq. (28) has lost the second-order spatial derivative, Eq. (26) cannot be fully satisfied and only the normal projection of the boundary conditions is kept. The fluid flow in this outer region can therefore be characterized by a velocity potential Φ_0 governed by the following system:

$$\frac{\partial^2\Phi_0}{\partial r^2} + \frac{1}{r}\frac{\partial\Phi_0}{\partial r} + \frac{1}{r^2}\frac{\partial^2\Phi_0}{\partial\theta^2} = 0 \tag{30}$$

$$\left.\frac{\partial\Phi_0}{\partial r}\right|_{r=1} = \dot{e}(t)\cos\theta, \qquad \left.\frac{\partial\Phi_0}{\partial r}\right|_{r=\alpha} = 0 \tag{31}$$

The solution of this system is readily obtainable by separation of variables; it is given by

$$\Phi_0(r,\theta,t) = -\frac{1}{\alpha^2-1}\left(r + \frac{\alpha^2}{r}\right)\dot{e}(t)\cos\theta \tag{32}$$

The nondimensional main-order velocity components far from the boundaries can then be deduced as follows:

$$u_0^r = \frac{1}{\alpha^2-1}\left(\frac{\alpha^2}{r^2} - 1\right)\dot{e}(t)\cos\theta \tag{33}$$

$$u_0^\theta = \frac{1}{\alpha^2-1}\left(\frac{\alpha^2}{r^2} + 1\right)\dot{e}(t)\sin\theta \tag{34}$$

where u_0^r and $u_0{}^\Phi$denote, respectively, the radial and azimuthal velocities.

3.3 Inner Resolution. Due to the no-slip boundary condition, a viscous boundary-layer is formed close to the moving cylinder. In this fluid part, the boundary layer variable $\eta=\beta^{1/2}(r-1)$ is injected into the Navier–Stokes equations. Moreover, the following inner expansion is performed for the nondimensional dependent variables

$$\begin{pmatrix}\bar{u}^\eta(\eta,\theta,t)\\ \bar{u}^\theta(\eta,\theta,t)\\ \bar{p}(\eta,\theta,t)\end{pmatrix} = \begin{pmatrix}0\\ \bar{u}_0^\theta(\eta,\theta,t)\\ \bar{p}_0(\eta,\theta,t)\end{pmatrix} + \beta^{-1/2}\begin{pmatrix}\bar{u}_1^\eta(\eta,\theta,t)\\ \bar{u}_1^\theta(\eta,\theta,t)\\ \bar{p}_1(\eta,\theta,t)\end{pmatrix} + \mathcal{O}(\beta^{-1}) \tag{35}$$

where $\bar{u}^\eta$, $\bar{u}^\theta$, and $\bar{p}$ are, respectively, the radial velocity, the azimuthal velocity, and the pressure in the boundary-layer. The introduction of the boundary-layer variable together with the inner expansion, Eq. (35), account for the different orders of magnitude of the radial and azimuthal boundary layer velocities: the radial velocity is normalized with the viscous diffusion velocity given by $\sqrt{\nu\omega}$ and the azimuthal velocity with the characteristic cylinder velocity. Introducing Eq. (35) into the Navier–Stokes equations and retaining the main-order terms yield the following system of equations:

$$\frac{\partial\bar{p}_0}{\partial\eta} = 0 \tag{36}$$

$$\frac{\partial\bar{u}_0}{\partial t} = -\frac{\partial\bar{p}_0}{\partial\theta} + \frac{\partial^2\bar{u}_0}{\partial\eta^2} \tag{37}$$

$$\frac{\partial\bar{u}_1^\eta}{\partial\eta} + \frac{\partial\bar{u}_0}{\partial\theta} = 0 \tag{38}$$

As expected, the unsteady and diffusion terms in Eq. (37) are now of the same order. Equation (36) states that the pressure at the main order is constant across the boundary layer. Therefore, the pressure term in Eq. (37) can be linked to the outer variables by considering the azimuthal component of Eq. (28) as follows:

$$-\frac{\partial\bar{p}_0}{\partial\theta} = \lim_{r\to1}\left(-\frac{1}{r}\frac{\partial p_0}{\partial\theta}\right) = \left.\frac{\partial u_0^\theta}{\partial t}\right|_{r=1} = \frac{\alpha^2+1}{\alpha^2-1}\ddot{e}(t)\sin\theta \tag{39}$$

Only the azimuthal boundary-layer velocity $\bar{u}_0^\theta$ is required for evaluation of the first-order fluid forces, since the inner radial velocity contributes to the higher-order terms. Thus, $\bar{u}_0^\theta$ must satisfy the no-slip boundary condition on the moving cylinder and must match the outer azimuthal velocity. It is fully characterized by the system

$$\frac{\partial\bar{u}_0}{\partial t} = \frac{\partial^2\bar{u}_0}{\partial\eta^2} + \frac{\alpha^2+1}{\alpha^2-1}\ddot{e}(t)\sin\theta \tag{40}$$

$$\bar{u}_0^\theta|_{\eta=0} = -\dot{e}(t)\sin\theta \tag{41}$$

$$\lim_{\eta\to\infty}\bar{u}_0^\theta = \frac{\alpha^2+1}{\alpha^2-1}\dot{e}(t)\sin\theta \tag{42}$$

Taking the Laplace transform of the above system, the inner azimuthal solution can be found in the Laplace domain,

$$\hat{u}_0^\theta(\eta,\theta,s) = \left(-\frac{2\alpha^2}{\alpha^2-1}e^{-\sqrt{s}\eta} + \frac{\alpha^2+1}{\alpha^2-1}\right)\frac{\hat{\dot{e}}(s)}{s}\sin\theta \tag{43}$$

where s is the Laplace variable and the circonflex denotes the Laplace transform of the corresponding temporal function.

3.4 Evaluation of Fluid Forces. The uniformly valid first-order dimensionless azimuthal velocity in the fluid domain is obtained by summing the inner and outer solutions (34) and (43) and removing the common limit (42), which is counted twice [24],

$$\hat{u}^\theta(r,\theta,s) = \left[\frac{1}{\alpha^2-1}\left(1+\frac{\alpha^2}{r^2}\right) - \frac{2\alpha^2}{\alpha^2-1}e^{-\sqrt{\beta}s(r-1)}\right]\frac{\hat{\dot{e}}(s)}{s}\sin\theta \tag{44}$$

The resultant dimensionless fluid forces on the inner cylinder can be evaluated in the Laplace domain by the formula [22]

$$\hat{\mathbf{F}}(s) = -\frac{1}{\pi}\int_0^{2\pi} \hat{p}|_{r=1}\mathbf{e_r}\,d\theta + \beta^{-1}\frac{1}{\pi}\int_0^{2\pi} (\nabla\hat{\mathbf{u}} + (\nabla\hat{\mathbf{u}})^T)|_{r=1}\cdot\mathbf{e_r}\,d\theta \tag{45}$$

The first term on the right-hand side can be expressed in terms of the fluid velocities, Eqs. (33) and (44), using integration by parts. Keeping only the main- and first-order terms in the power expansion of $\beta^{-1/2}$ gives the integrated fluid forces in the Laplace domain. The nondimensional fluid forces in the temporal domain can then be found by using the convolution theorem and some inverse Laplace transform properties. Only the $\mathbf{e_x}$-component of $\mathbf{F}$ is nonzero and is given by

$$\varphi(t) = -\frac{\alpha^2+1}{\alpha-1}\ddot{e}(t) - \beta^{-1/2}\frac{\alpha^2}{\alpha^2-1}\frac{4}{\sqrt{\pi}}\int_0^t \frac{\ddot{e}(\tau)}{\sqrt{t-\tau}}d\tau \tag{46}$$

The first term is the small amplitude potential added mass effect found in the previous section. The second one, inversely proportional to the square root of the Stokes number, is the first-order viscous rectification. The total history of the imposed motion is involved so that its effect can be attributed neither to added mass nor viscous damping alone. The convolution product kernel, known explicitly, indicates that the imposed motion at time τ has decreasing influence on the fluid forces at time t as $t-\tau$ increases. This type of convolution product (which accounts for viscous effects) is well known and can be found in Ref. [25] for an infinite plate. For an infinite fluid domain, the resulting dimensionless fluid forces are then given by

$$\varphi(t) = -\ddot{e}(t) - \beta^{-1/2}\frac{4}{\sqrt{\pi}}\int_0^t \frac{\ddot{e}(\tau)}{\sqrt{t-\tau}}d\tau \tag{47}$$

which consists of the displaced fluid term and a first-order viscous correction. This expression can also be found, with higher-order viscous corrections, from existing harmonic models [26,27] based on a Fourier transform method [28]. Nevertheless, for relatively high Stokes number flows, the first-order term suffices to account for the viscous effects [29].

4 Compressible Model

4.1 Problem Formulation. Here, small amplitude motions of the inner circular cylinder in an inviscid compressible fluid are considered. The solution of the associated harmonic problem can be found in Ref. [2], for instance. The fluid dynamics is assumed to be governed by the wave equation for the velocity potential

$$\nabla^2\Phi - \Omega^2\frac{\partial^2\Phi}{\partial t^2} = 0 \tag{48}$$

where the variables are normalized according to Table 1 and the compressibility number Ω appears explicitly. The boundary conditions are of Neumann type and can be written as

$$\left.\frac{\partial\Phi}{\partial r}\right|_{r=1} = \dot{e}(t)\cos\theta, \qquad \left.\frac{\partial\Phi}{\partial r}\right|_{r=\alpha} = 0 \tag{49}$$

4.2 Evaluation of Fluid Forces. The system of Eqs. (48) and (49) can be solved by using the Laplace transform for the temporal variable and performing a separation of variables. The resulting nondimensional velocity potential in the Laplace domain is then given by

$$\hat{\Phi}(r,\theta,s) = \frac{\hat{\dot{e}}(s)}{ks}\frac{Y_1'(\alpha k)J_1(kr) - J_1'(\alpha k)Y_1(kr)}{Y_1'(\alpha k)J_1'(k) - Y_1'(k)J_1'(\alpha k)}\cos\theta \tag{50}$$

where $k=i\Omega s$, the circonflex denotes the Laplace transform. Here, J_1 and Y_1 are the Bessel functions of order 1, respectively, of the first and second kinds. The prime denotes the derivative according to the function argument. Making use of Eq. (50) and applying the convolution theorem yield the nondimensional $\mathbf{e_x}$-component of the fluid forces in the temporal domain as follows:

$$\varphi(t) = -\int_0^t C(t-\tau)\ddot{e}(\tau)d\tau \tag{51}$$

where the kernel $C(t)$ must be evaluated. This requires a Laplace inversion according to a contour integration based on the Bromwich integral as follows:

$$C(t) = \frac{1}{2\pi i}\int_{\sigma-i\infty}^{\sigma+i\infty}\hat{C}(s)e^{st}ds \tag{52}$$

with

$$\hat{C}(s) = -\frac{1}{k}\frac{Y_1'(\alpha k)J_1(k) - J_1'(\alpha k)Y_1(k)}{Y_1'(\alpha k)J_1'(k) - Y_1'(k)J_1'(\alpha k)} \tag{53}$$

This inversion can be obtained numerically. Figure 2 shows the temporal evolution of the kernel $C(t)$ for $\Omega=1$ and a few different values of α. These functions have points of finite discontinuity that account for the reflections of hydrodynamic waves in the fluid domain. The intervals between the discontinuities are equal to the time for a wave to travel from the inner to the outer cylinder and back. For instance, for $\Omega=1$ and $\alpha=2$, the pressure wave induced by the impulse motion of the inner cylinder at $t=0$ is reflected back on the outer cylinder at $t=1$ and influences the integrated fluid forces on the inner cylinder at $t=2$. Furthermore, the more confined the fluid domain is, the more discontinuities the kernel contains. At the beginning of the process, that is, before the wave returns to the inner cylinder, the kernel is seen to be independent of the confinement ratio α. In evaluating the fluid forces at a time t in a confined domain, the motion of the inner cylinder at an early time τ is as important as that at time t, even if $t-\tau$ is large. On the other hand, for an infinite fluid domain, the motion at large $t-\tau$ does not significantly influence the fluid forces at t, since the waves are not reflected back.

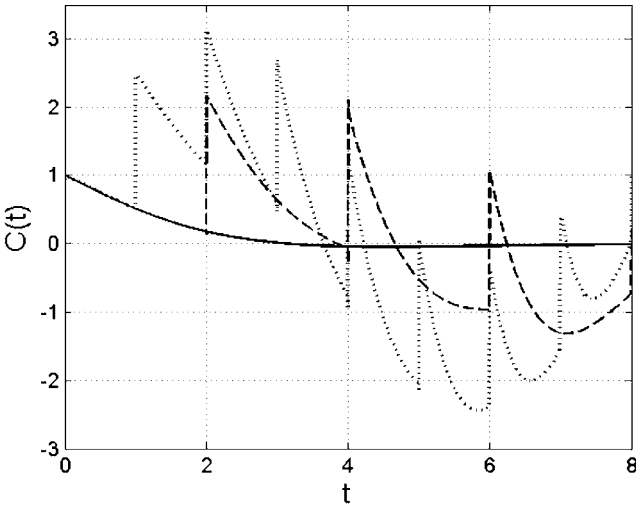

Fig. 2 Evolution of the compressible fluid forces kernel with $\Omega=1$, for different confinement numbers α: (···) 1.5, (– – –) 2, and (—) 10

5 Fluid Forces on a Rigid Circular Cylinder Subjected to a Sine-Wave Shock

5.1 Sine-Wave Shock. The fluid forces obtained in Secs. 2–4 are illustrated and compared for a specific motion imposed on the inner cylinder that corresponds to a unique sinusoidal period of acceleration and is then stopped. Hence, the dimensional motion is fully determined by

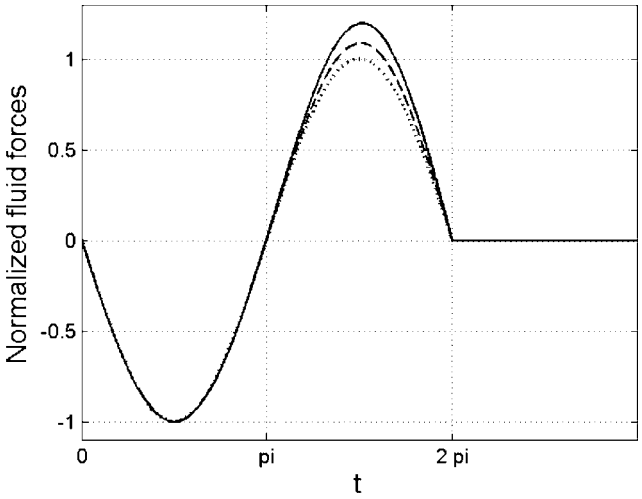

Fig. 3 Evolution of the nondimensional fluid forces normalized with the maximum of the Fritz fluid force model [19] for α=2. Comparison between the Fritz model (···) and the non-negligible displacement model for different Keulegan–Carpenter numbers λ: (– – –) 0.19 and (—) 0.28

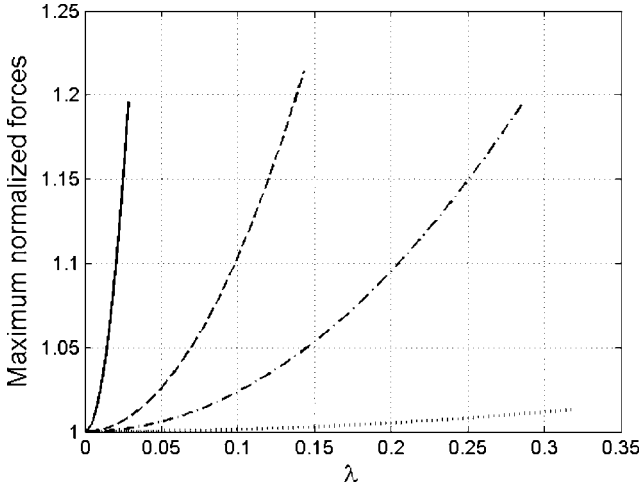

Fig. 4 Maximum nondimensional fluid forces, obtained with the non-negligible displacement model and normalized with the maximum of the Fritz fluid force model [19], in function of the Keulegan–Carpenter number and for different confinement numbers α: (···) 4, (–·–) 2, (– – –) 1.5 and (—) 1.1

$$\ddot{e}(t)=\begin{cases}\dfrac{U\omega}{2}\sin\omega t, & \forall t\in[0,2\pi/\omega]\\ 0, & \forall t>2\pi/\omega\end{cases} \tag{54}$$

where ω is the pulsation of the shock. In what follows, it is also convenient to express this motion in a nondimensional form. Using the normalization factor of Table 1 yields the simple representation

$$\ddot{e}(t)=\begin{cases}\dfrac{1}{2}\sin t, & \forall t\in[0,2\pi]\\ 0, & \forall t>2\pi\end{cases} \tag{55}$$

Even if this function is partly composed of a harmonic function, it can be considered as a purely transient motion since it starts from rest at t=0 and stops at t=2π. It consists of a simple imposed translation and is representative of the early residual motion undergone by equipment during shock loading.

5.2 Non-Negligible Amplitude Motion Effects. Here, the dimensionless fluid forces given by Eq. (23) are illustrated on the specific imposed motion defined by Eq. (55). Figure 3 shows the temporal evolution of these forces with confinement number α =2 for different Keulegan–Carpenter numbers λ. They are normalized with the maximum value given by the potential Fritz model [19], which assumes negligible amplitude motions. It can be seen that the nonlinear and Fritz models predict similar forces when the inner cylinder is still close to its initial position, but show different behaviors as the inner cylinder approaches the outer one. This results in a force increase that becomes more significant as the Keulegan–Carpenter number increases. This effect is checked with a finite-volume numerical code able to take into account moving boundaries [30]. The nonlinear model is in good agreement with these numerical results for inner-cylinder displacements up to 60% of the radial clearance. Some discrepancies are observed for higher displacements. More specifically, the nonlinear model underestimates the maximum fluid forces, and hence more than three terms should be kept in Eq. (19) to reproduce the strong geometrical deformation. Nevertheless, the nonlinear model predicts the trend better than the Fritz model.

Figure 4 shows the maximum fluid forces obtained with the nonlinear model as function of the Keulegan–Carpenter number λ for different confinement numbers α, and also normalized by the maximum Fritz model forces. At a given λ, the more confined the fluid domain, the greater the discrepancies with the Fritz model, becoming as much as 20% for $\alpha\leqslant$2. The different limits of the curves in Fig. 4 can be explained by recalling that the nonlinear model was derived assuming an inner-cylinder displacement smaller than its radius and smaller than the radial clearance.

5.3 Viscous Effects. Here, the viscous fluid force model given by Eq. (46) is applied to the specific motion of Eq. (55). The temporal evolution normalized by the maximum potential forces is displayed in Fig. 5 with confinement number α=2 for different Stokes numbers β. Viscous effects are shown to increase the fluid forces on the inner cylinder and to induce a residual fluid force that tends quite rapidly to zero once the cylinder stops. These effects are in good agreement with the numerical simulations on an infinite fluid domain in Ref. [29]. For a confined fluid domain, these results are expected to be valid when the boundary layer is much thinner than the radial clearance, that is, for very low Keulegan–Carpenter numbers and for cases where $\sqrt{\nu/\omega}\ll R_2$

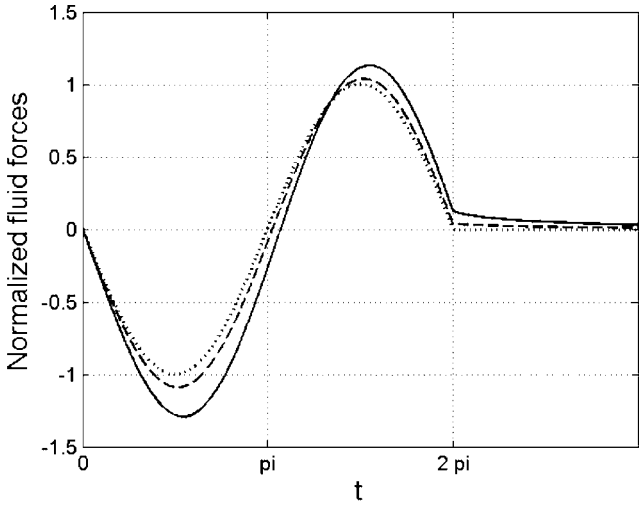

Fig. 5 Evolution of the nondimensional fluid forces normalized with the maximum of the Fritz fluid force model [19] for α=2. Comparison between the Fritz model (···) and the viscous model for different β: (– – –) 500 and (—) 50.

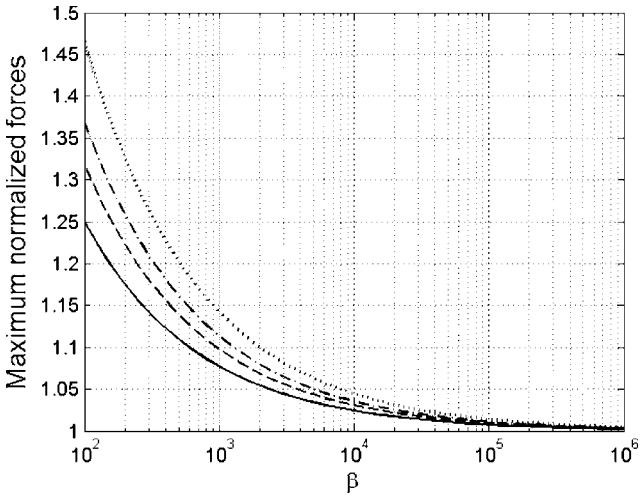

Fig. 6 Maximum nondimensional fluid forces, obtained with the viscous model and normalized with the maximum of the Fritz fluid force model [19], in function of the Stokes number and for different confinement numbers α: (⋯) ∞, (–·–) 2, (– – –) 1.5 and (—) 1.1

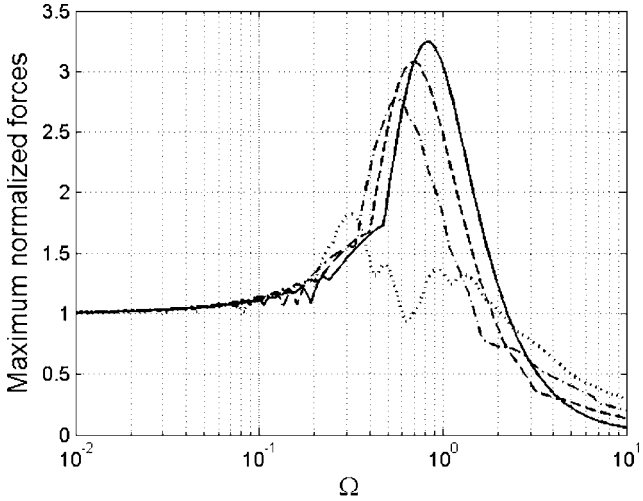

Fig. 8 Maximum nondimensional fluid forces, obtained with the compressible model and normalized with the maximum of the Fritz fluid force model [19], in function of the compressibility number and for different confinement numbers α: (⋯) 4, (–·–) 2, (– – –) 1.5 and (—) 1.1

$-R_1$ (or, in dimensionless form, $\beta^{1/2}(\alpha-1)\gg 1$).

The maximum fluid forces normalized by the maximum potential forces as function of the Stokes number are illustrated in Fig. 6 for different confinement numbers. Large discrepancies are observed for low Stokes numbers, an effect that is less pronounced for confined domains. This is because the potential added mass increases more rapidly with the confinement than the viscous term. This result is not expected to be valid for strongly confined domains in which viscous forces become predominant.

5.4 Compressible Effects. The compressible fluid forces of Eq. (51) are now applied to the specific motion described through Eq. (55). The temporal evolution, normalized by the maximum potential forces, is shown in Fig. 7 for $\alpha=2$ and different compressible numbers Ω. It can be seen that compressible waves are generated in the fluid domain and result in fluid force oscillation around the potential curve due to their multiple reflections on the boundaries. Once the inner cylinder has been stopped, the compressible waves continue to induce these harmonic oscillations without damping. For higher compressible numbers than those in Fig. 7, several compressible waves can be generated and clearly identified on a single curve. In an infinite fluid domain, the loss of energy induced by the outgoing waves has a damping effect [2].

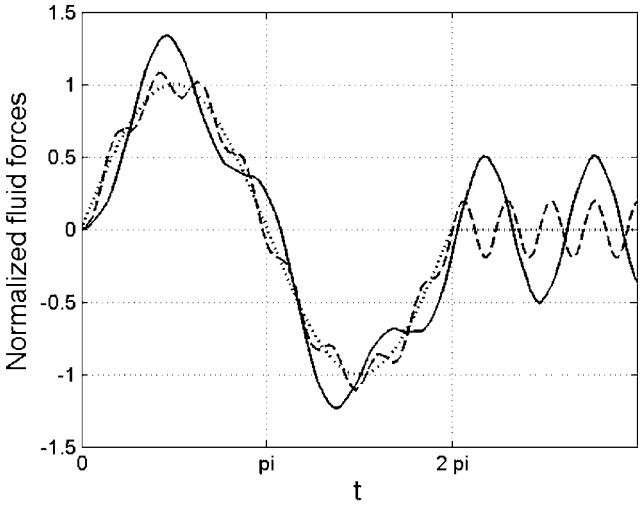

Fig. 7 Evolution of the nondimensional fluid forces normalized with the maximum of the Fritz fluid force model [19] for $\alpha=2$. Comparison between the Fritz model (⋯) and the compressible model for different Ω: (– – –) 0.08 and (—) 0.2.

The maximum fluid forces normalized by the maximum potential value are displayed in Fig. 8 as function of the compressible number Ω and different confinement numbers α. For small compressible numbers, the fluid forces tend to their potential value for all confinements. For large compressible numbers, they tend to zero due to the increasing difference between the imposed motion frequency and the fundamental fluid cavity acoustic frequency. Pseudoresonances are observed around $\Omega\approx 1$. This effect is all the more pronounced as the domain becomes more and more confined. The maximum fluid forces are then seen to be three times greater than their corresponding potential value. Several peaks on the curve $\alpha=4$ can be observed, a reminder that a compressible fluid domain cannot be viewed as a single-degree-of-freedom spring-mass system since its harmonic dynamics contains an infinite number of resonant frequencies [2].

5.5 Illustration of the Use of the Models on a Given System. The three models were described independently in Secs. 2–4 as a function of their corresponding dimensionless numbers. They can, however, be grouped on a single figure for a particular geometry, so that their range of validity can be discussed and the significant fluid effects in a particular case can be identified. For instance, by fixing the geometrical parameters R_1 and R_2, the fluid viscosity ν, the speed of sound c, and the imposed velocity U, the maximum normalized forces can be displayed as a function of the dimensional imposed pulsation ω. Hence, increasing ω causes the Stokes number and the compressibilty number increase and the Keulegan–Carpenter number decrease. Such curves are given in Fig. 9 with $R_1=0.2$ m, $U=0.5$ m s^{-1}, $c=1500$ m s^{-1}, $\nu=10^{-6}$ m^2 s^{-1}, and several R_2. For imposed pulsations such that $\omega\leqslant 1$ s^{-1}, viscous effects must be taken into account. For 1 s$^{-1}\leqslant\omega\leqslant 10^2$ s^{-1}, the flow is dominated by potential effects and for 10^2 s$^{-1}\leqslant\omega\leqslant 10^5$ s^{-1}, fluid compressibility must be considered.

6 Conclusion

Transient fluid loading on a circular cylinder moving along a radial line is addressed. The fluid domain can be infinite or cylindrically confined. A nonlinear fluid force model that takes into account the geometrical deformation and fluid advection is de-

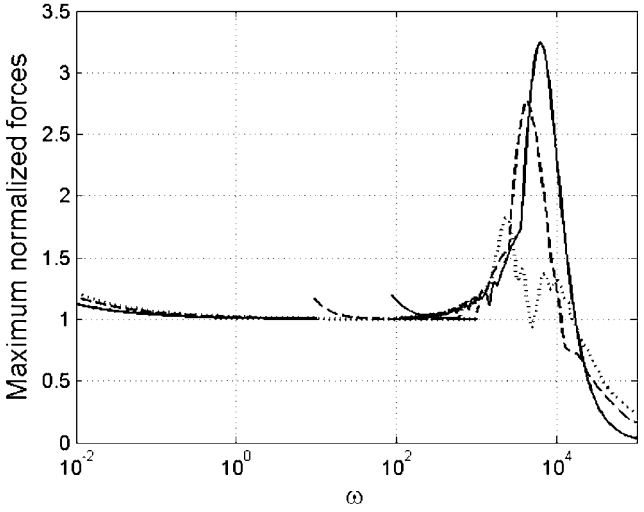

Fig. 9 Maximum fluid forces obtained with the different models and normalized with the maximum of the Fritz fluid force model [19], in function of the dimensional imposed motion pulsation, for different confinement numbers α: (⋯) 4, (– – –) 2, and (—) 1.1

rived. Nonlinear effects are shown to be dependent on the square of the Keulegan–Carpenter number λ. Models of the viscous and compressible fluid forces take the form of convolution products including the history of the imposed acceleration. Their kernels are linked to the viscous and compressible waves propagating in the fluid domain. Viscous effects are shown to be inversely proportional to the square root of the Stokes number β and the compressible effects to be dependent on the compressibility number Ω. All of these models are illustrated for a specific imposed motion that is representative of the early residual motion felt by internal naval components during shock loading. The temporal evolution of the fluid forces is then described for different values of the dimensionless parameters and the maximum fluid force curves are displayed as a function of these dimensionless parameters. Lastly, the models are examined all together for a particular case and are shown to cover a broad range of motions. Thus, for a given geometry and imposed displacement, the appropriate fluid model can be identified and the resulting fluid forces rapidly estimated.

All of these models emphasize some fluid effects in simple asymptotic cases. However, all physical phenomena are of course not treated in this paper. For instance, large-displacement motions in a potential flow and viscous effects are handled independently, and this prevents the models from tackling boundary-layer separation issues. Furthermore, the viscous fluid forces are derived by assuming laminar flow. This assumption does not hold for high-Stokes-number flows, even at very low Keulegan–Carpenter numbers, due to the presence of centrifugal hydrodynamic instabilities [31,32] in the boundary layer. In harmonic flows, these three-dimensional phenomena are known to increase the fluid damping [33,34] by a factor 2. Another restriction comes from the monophasic assumption, which makes the models incapable of accounting for cavitation phenomena. The present paper gives, however, general guidance that can be used by design engineers for the purpose of estimating the fluid force level and, if required, selecting the meaningful fluid model to use in further investigation.

References

[1] Gibert, R., 1986, *Vibrations des Structures. Interaction Avec les Fluides. Sources d'Excitation Aléatoires* (Collection de la Direction des Etudes et Recherches d'Electricité de France Vol. 69), Eyrolles, Paris.

[2] Chen, S.-S., 1987, *Flow Induced Vibrations*, Hemisphere, Washington, DC.

[3] Habault, D., and Filippi, P., 2003, "On the Transient Response of a Fluid-Loaded Structure Represented by a Series of Resonances Modes," J. Sound Vib., **259**, pp. 1269–1275.

[4] Habault, D., and Filippi, P., 2004, "A Numerical Method for the Computation of the Resonance Frequencies and Modes of a Fluid-Loaded Plate: Application to the Transient Response of the System," J. Sound Vib., **270**, pp. 207–231.

[5] Stepanishen, P., 1997, "Transient Vibratory Response of Fluid-Loaded Structures Using Convolution Integral Equations," J. Acoust. Soc. Am., **101**, pp. 1877–1889.

[6] Axisa, F., and Antunes, J., 2006, *Modelling of Mechanical Systems—Fluid-Structure Interaction*, Elsevier, New York.

[7] Iakovlev, S., 2002, "Interaction of a Spherical Shock Wave and a Submerged Fluid-Filled Circular Cylindrical Shell," J. Sound Vib., **255**, pp. 615–633.

[8] Iakovlev, S., 2004, "Influence of a Rigid Coaxial Core on the Stress-Strain State of a Submerged Fluid-Filled Circular Cylindrical Shell Subjected to a Shock Wave," J. Fluids Struct., **19**, pp. 957–984.

[9] El-Shafei, A., and Crandall, S., 1991, "Fluid Inertia Forces in Squeeze Film Dampers," ASME Rotating Machinery and Vehicle Dynamics, Vol. 35, pp. 219–228.

[10] Tiehy, J., and Bou-Saïd, B., 1991, "Hydrodynamic Lubrification and Bearing Behavior With Impulsive Loads," STLE Tribol. Trans., **34**, pp. 505–512.

[11] Han, Y., and Rogers, R., 2001, "Nonlinear Fluid Forces in Cylindrical Squeeze Films. Part I: Short and Long Lengths," J. Fluids Struct., **15**, pp. 151–169.

[12] Usha, R., and Vimala, P., 2003, "Squeeze Film Force Using an Elliptical Velocity Profile," ASME J. Appl. Mech., **70**, pp. 137–142.

[13] Lu, Y., and Rogers, R., 1995, "Instantaneous Squeeze Film Force Between a Heat Exchanger Tube With Arbitrary Tube Motion and a Support Plate," J. Fluids Struct., **9**, pp. 835–860.

[14] Zhou, T., and Rogers, R., 1997, "Simulation of Two-Dimensional Squeeze Film and Solid Contact Forces Acting on a Heat Exchanger Tube," J. Sound Vib., **203**, pp. 621–639.

[15] Schlichting, H., 1979, *Boundary Layer Theory*, 7th ed., McGraw-Hill, New York.

[16] Sarpkaya, T., 1986, "Force on a Circular Cylinder in Viscous Oscillatory Flow at Low Keulegan–Carpenter Numbers," J. Fluid Mech., **165**, pp. 61–71.

[17] Koumoutsakos, P., and Leonard, A., 1995, "High Resolution Simulations of the Flow Around an Impulsively Started Circular Cylinder Using Vortex Methods," J. Fluid Mech., **296**, pp. 1–38.

[18] Pettigrew, M., and Taylor, C., 2004, "Damping of Heat Exchanger Tubes in Two-Phase Flow: Review and Design Guidelines," ASME J. Pressure Vessel Technol., **126**, pp. 523–533.

[19] Fritz, R., 1972, "The Effects of Liquids on the Dynamic Motion of Immersed Solids," J. Eng. Ind., Trans ASME, **94**, pp. 167–173.

[20] Van Dyke, M., 1964, *Perturbation Methods in Fluid Mechanics*, Academic, New York.

[21] Leblond, C., Sigrist, J.-F., Lainé, C., Auvity, B., and Peerhossaini, H., 2006, "Fluid Forces on a Circular Cylinder Moving Transversely in Cylindrical Confinement: Extension of the Fritz Model to Larger Amplitude Motions," *Proceedings of ASME, P.V.P.*, Vancouver, Canada, ICPVT11-93051.

[22] Batchelor, G., 1997, *An Introduction to Fluid Dynamics*, Cambridge University Press, Cambridge.

[23] Stokes, G., 1851, "On the Effect of the Internal Friction of Fluids on the Motion of Pendulums," Trans. Cambridge Philos. Soc., **9**, pp. 8–106.

[24] Kervokian, J., and Cole, J., 1996, *Multiple Scale and Singular Perturbation Methods*, Springer, New York.

[25] Lamb, H., 1932, *Hydrodynamics*, 6th ed., Cambridge University Press, Cambridge.

[26] Wang, C., 1968, "On High Frequency Oscillatory Viscous Flow," J. Fluid Mech., **32**, pp. 55–68.

[27] Mélot, V., Sigrist, J.-F., Lainé, C., Auvity, B., and Peerhossaini, H., 2006, "Fluid Forces on a Moving Body at Low Amplitude in Fluid at Rest. Part 1. A Review of Literature," in *Proceedings of ASME, P.V.P.*, Vancouver, Canada, ICPVT11-93018.

[28] Landau, L., and Lifshitz, E., 1987, *Course of Theoretical Physics, Fluid Mechanics*, Pergamon, New York.

[29] Mélot, V., Sigrist, J.-F., Lainé, C., Auvity, B., and Peerhossaini, H., 2006, "Fluid Forces on a Moving Body at Low Amplitude in Fluid at Rest. Part 2. Analytical and Numerical Study for an Accelerated Circular Cylinder," in *Proceedings of ASME, P.V.P.*, Vancouver, Canada, ICPVT11-93016.

[30] Mélot, V., Leblond, C., Sigrist, J.-F., Lainé, C., Auvity, B., and Peerhossaini, H., 2006, "Fluid Forces on a Circular Cylinder Subjected to a Transient Motion at Low Amplitude in Infinite Medium and in Cylindrical Confinement," *Proceedings of ASME, Joint US-European Fluids Engineering Division Summer Meeting*, Miami, FL.

[31] Honji, H., 1981, "Streaked Flow Around an Oscillating Circular Cylinder," J. Fluid Mech., **107**, pp. 507–520.

[32] Hall, P., 1983, "On the Stability of Unsteady Boundary Layer on a Cylinder Oscillating Transversely in a Viscous Flow," J. Fluid Mech., **146**, pp. 337–367.

[33] Sarpkaya, T., 2001, "Hydrodynamic Damping and Quasi-Coherent Structures at Large Stokes Numbers," J. Fluids Struct., **15**, pp. 909–928.

[34] Sarpkaya, T., 2002, "Experiments on the Stability of Sinusoidal Flow Over a Circular Cylinder," J. Fluid Mech., **457**, pp. 157–180.